AD-A121 775 FATIGUE MICROCRACK BEHAVIOR UNDER THE INFLUENCE OF SURFACE RESIDUAL STRESSES(U) SOUTHWEST RESEARCH INST SAN ANTONIO TX J E HACK ET AL. 01 NOV 82 1/1

UNCLASSIFIED N00014-78-C-0674 F/G 20/11 NL

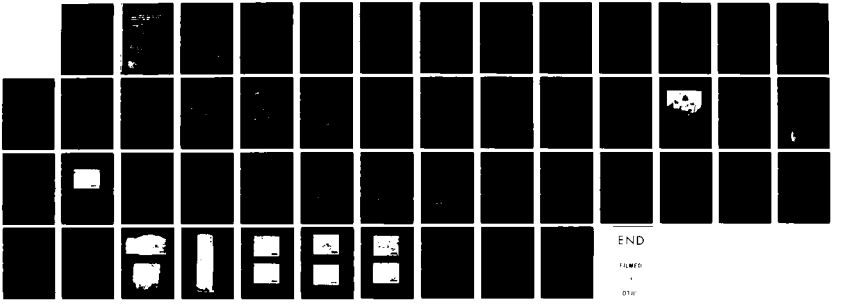

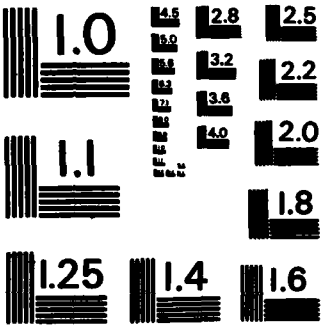

MICROCOPY RESOLUTION TEST CHART
NATIONAL BUREAU OF STANDARDS - 1963 - A

[redacted]

[redacted]

[redacted] RESEARCH INSTITUTE
[redacted] HOUSTON

(12)

FATIGUE MICROCRACK BEHAVIOR UNDER THE INFLUENCE OF SURFACE RESIDUAL STRESSES

J. E. Hack and G. R. Leverant
Southwest Research Institute
P. O. Drawer 28510
San Antonio, Texas 78284

INTERIM REPORT For Period September 1, 1981 — August 31, 1982
Contract N00014-78-C-0674

Prepared for
OFFICE OF NAVAL RESEARCH
800 North Quincy Street
Arlington, Virginia 22217

November 1, 1982

Approved:

U. S. Lindholm, Director
Department of Materials Sciences

UNCLASSIFIED
SECURITY CLASSIFICATION OF THIS PAGE (When Data Entered)

REPORT DOCUMENTATION PAGE

READ INSTRUCTIONS BEFORE COMPLETING FORM

1. REPORT NUMBER	2. GOVT ACCESSION NO. AD-A121775
3. RECIPIENT'S CATALOG NUMBER	
4. TITLE (and Subtitle) FATIGUE MICROCRACK BEHAVIOR UNDER THE INFLUENCE OF SURFACE RESIDUAL STRESSES	5. TYPE OF REPORT & PERIOD COVERED Interim Report Sept. 1, 1981-Aug. 31, 1982
	6. PERFORMING ORG. REPORT NUMBER 06-5382/4
7. AUTHOR(s) J. E. Hack, G. R. Leverant	8. CONTRACT OR GRANT NUMBER(s) N00014-78-C-0674
9. PERFORMING ORGANIZATION NAME AND ADDRESS Southwest Research Institute, P. O. Drawer 28510, San Antonio, Texas 78284	10. PROGRAM ELEMENT, PROJECT, TASK AREA & WORK UNIT NUMBERS Project Element 122201 NR031-812/6-23-78(471)
11. CONTROLLING OFFICE NAME AND ADDRESS Office of Naval Research, 800 North Quincy Street, Arlington, Virginia 22217	12. REPORT DATE November 1, 1982
	13. NUMBER OF PAGES 42 + prelims
14. MONITORING AGENCY NAME & ADDRESS(if different from Controlling Office)	15. SECURITY CLASS. (of this report) UNCLASSIFIED
	15a. DECLASSIFICATION/DOWNGRADING SCHEDULE

16. DISTRIBUTION STATEMENT (of this Report)

Reproduction in whole or in part is permitted for any purpose of the United States Government. Distribution is unlimited.

17. DISTRIBUTION STATEMENT (of the abstract entered in Block 20, if different from Report)

18. SUPPLEMENTARY NOTES

19. KEY WORDS (Continue on reverse side if necessary and identify by block number)

Fatigue	Titanium	Crack Growth
Microcrack	HY-130 Steel	Boundary Integral
Residual Stress	Surface Crack Opening Displacement	Technique
Brine Environment	Stress Intensity	Weld Microstructure

20. ABSTRACT (Continue on reverse side if necessary and identify by block number)

The boundary integral technique has been used to calculate complete crack opening profiles under conditions of zero and compressive surface residual stress states. The results show that in addition to reducing the overall opening of the crack during loading, a compressive surface residual stress can induce a lenticular crack profile through-the-thickness of the material. The boundary integral calculations also provided excellent correlation with observed SCOD behavior. These results lend a great deal of credibility to

DD FORM 1 JAN 73 1473 EDITION OF 1 NOV 65 IS OBSOLETE

UNCLASSIFIED
SECURITY CLASSIFICATION OF THIS PAGE (When Data Entered)

the boundary integral stress intensity factor calculations.

Direct observation of SCOD behavior and growth rate measurements on microcracks in HY-130 steel in both air and an aqueous solution of 3.5% NaCl indicate that residual stresses reduce SCOD much in the same way as in Ti alloys. In addition to this purely mechanical affect, the compressive residual stress induced lenticular crack profile apparently disrupts the crack tip chemistry in a brine environment and eliminates the crack growth acceleration due to the so called small crack effect. A possible mechanism for this is discussed.

The results of preliminary optical metallography of the microstructural development in three types of welding processes for one inch thick plate of Ti-6Al-2Nb-1Ta-0.8Mo are also presented.

FOREWORD

The research reported herein was conducted by Southwest Research Institute of San Antonio, Texas, under Contract N00014-78-C-0674. The report summarizes work accomplished during the period September 1981 through August 1982. Dr. Bruce MacDonald was the ONR Program Manager. The work was conducted under the general supervision of Dr. Gerald R. Leverant, SwRI Project Manager, with assistance from Mr. John E. Hack, who acted as Principal Scientist. Special acknowledgement is due to Drs. David L. Davidson and Robert Sherman, who assisted with the in-situ loading experiments in the SwRI SEM and Dr. Kwai S. Chan and Mr. Joseph W. Cardinal, who performed the crack profile calculations with 3-D BINTEQ. The helpful comments of Dr. Richard A. Page and Mr. Stephen J. Hudak and the technical support of Messrs. Harold Saldana and Kyle Short are also greatly appreciated.

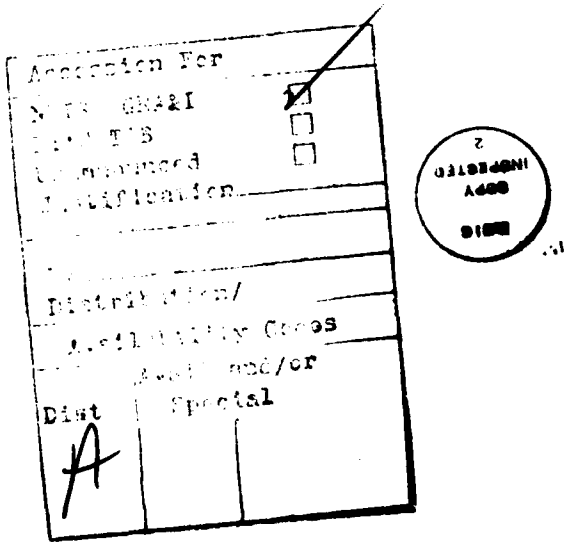

TABLE OF CONTENTS

LIST OF TABLES

LIST OF FIGURES

I. INTRODUCTION

Residual stresses are introduced in metal surfaces by many common mechanical and thermal processes. Their introduction can be intentional, as in the case of shot peening, or inadvertent, as in the case of differential contraction between weld metal and base metal during solidification and cooldown. The affected region due to shot peening is generally quite thin with a maximum depth of 125-250 μm, while welding-induced residual stresses can extend to significant depths in the material. Since fatigue crack initiation in metals generally occurs at or near a free surface and the initial growth rates of microcracks are in the near-threshold region ($\approx 10^{-6}$ mm/cycle), fatigue cracks spend a significant portion of their lifetimes under the influence of the surface residual stress state. In addition, aggressive environments can dramatically change crack growth behavior in the near-threshold region, either acting alone or in conjunction with an imposed surface residual stress state. This report details the current results of an ongoing program to quantify the relationship between surface condition, environment and fatigue microcrack opening and growth behavior.

The approach utilized in this program is to quantify the effects of surface residual stresses and environment on surface crack opening displacement (SCOD) behavior. Since COD can be directly related to crack growth rate [1,2], these data can be used to correlate these parameters with fatigue behavior. A loading stage which operates in-situ in an SEM has been used to generate SCOD vs. load data for microcracks in Ti-6Al-4V and HY-130 steels.

Current results of experimental observations are presented herein that compare SCOD and crack growth behavior in HY-130 steel in the presence of various levels of compressive stress. In addition, SCOD and crack growth behavior are compared for air and aqueous brine environments. A previously developed analytical approach for the prediction of SCOD behavior has been applied to cracked steel specimens which are free of compressive surface residual stresses. Furthermore, crack profiles in Ti-6Al-4V specimens under the influence of surface residual stresses have been calculated by the boundary integral technique and give excellent agreement with direct SCOD measurements. The lenticular through-the-thickness crack opening behavior predicted by the calculations for the titanium alloy specimens has also been used to qualitatively explain the behavior of surface microcracks in HY-130 steel under the influence of a surface residual stress and brine environment. Preliminary microstructural information on fusion and heat-affected zones in one inch thick weldments of Ti-6Al-2Nb-1Ta-0.8Mo produced by three different welding procedures is also reported.

II. PREDICTION OF SCOD BEHAVIOR IN THE PRESENCE OF A RESIDUAL STRESS GRADIENT

A. Background

A detailed description of the closed form analytical approach developed for the prediction of SCOD behavior of surface cracks has been given previously [3]. In general, it was found that the approach gave excellent correlation between predicted and observed SCOD behavior for Mode I surface macrocracks, corner cracks, and surface microcracks when no surface residual stresses were present. The approach was found to work in both Ti-6Al-4V and 4140 steel. The presence of a residual stress gradient produced an overestimation of crack opening with load. This problem has been solved by calculating the crack opening displacement behavior through-the-thickness of the specimen using a computer program based on the boundary integral technique (3-D BINTEQ). A description of this solution will be given below while the application of the closed form solution to HY-130 steel will be described in Section III.

As mentioned above, the results described in [3], for corner cracks in Ti-6Al-4V, show that the analytical approach used in this program overpredicts crack opening with load when a near-surface residual compressive stress gradient is present. The approach is based on combining an expression for the displacement of a part-through crack due to Irwin [4] with values of the surface crack tip stress intensity factor obtained from a computer program called BIGIF (Boundary Integral Generated Influence Functions) [5]. The BIGIF program calculates a "global" stress intensity factor for each position by integrating over the crack front. Thus, the

constraints introduced by a three-dimensional part-through crack and an imposed gradient in stress across the crack are readily handled. Theoretically, then, the stress intensity factors calculated by BIGIF when residual stresses are present should still be appropriate.

Table I shows a comparison of predictions based on the closed form solution and observed SCOD behavior for corner cracks in Ti-6Al-4V with and without the presence of the compressive surface residual stress gradients shown in Figure 1. As can be seen from the data, the closed form solution overpredicts the SCOD at the midpoint of the front face of the crack by about a factor of two in the presence of a residual stress. This occurs even though the K values were corrected to include the near-surface residual stress state. Assuming that the K values are correct, the logical source of the discrepancy was felt to be the opening expression itself. The opening expression was derived based upon the crack opening as a semi-ellipse. Thus, the crack profile is constrained to follow a prescribed elliptical path for a given loading condition and crack geometry. If the applied stress is not uniform, as in the case of the near-surface compressive residual stress gradient imposed on the corner cracks, the results indicate that the crack can close down more at the surface that at some point underneath the surface. This is due to the fact that the buried crack tip, if it has grown into a region of reduced compressive residual stress, is only influenced by the higher level of residual stress in the near-surface region through the constraints introduced by the semi-elliptical crack geometry. In this instance, the buried crack tip may open to a significant fraction of the elastic opening which it would have had

TABLE I

CORRELATION OF MEASURED AND PREDICTED MODE I CORNER CRACK SCOD
AT MAXIMUM LOAD WITH A COMPRESSIVE RESIDUAL STRESS STATE
USING CLOSED FORM SOLUTION

Sample	Crack Length on Front Face (μm)	Crack Length on Side Face (μm)	Surface Residual Stress Value	Maximum Stress (MPa)	K_s (MPa$\sqrt{m}$)	Predicted SCOD (μ)	Measured SCOD (μ)
Ti-2	1300	650	-560	500	10.1	6.0	3.8
Ti-6	1200	750	-860	560	9.6	5.5	3.1
Ti-6†	1200	750	≈0	560	21.5	11.2	11.3

† Stress relieved after initial experiment.

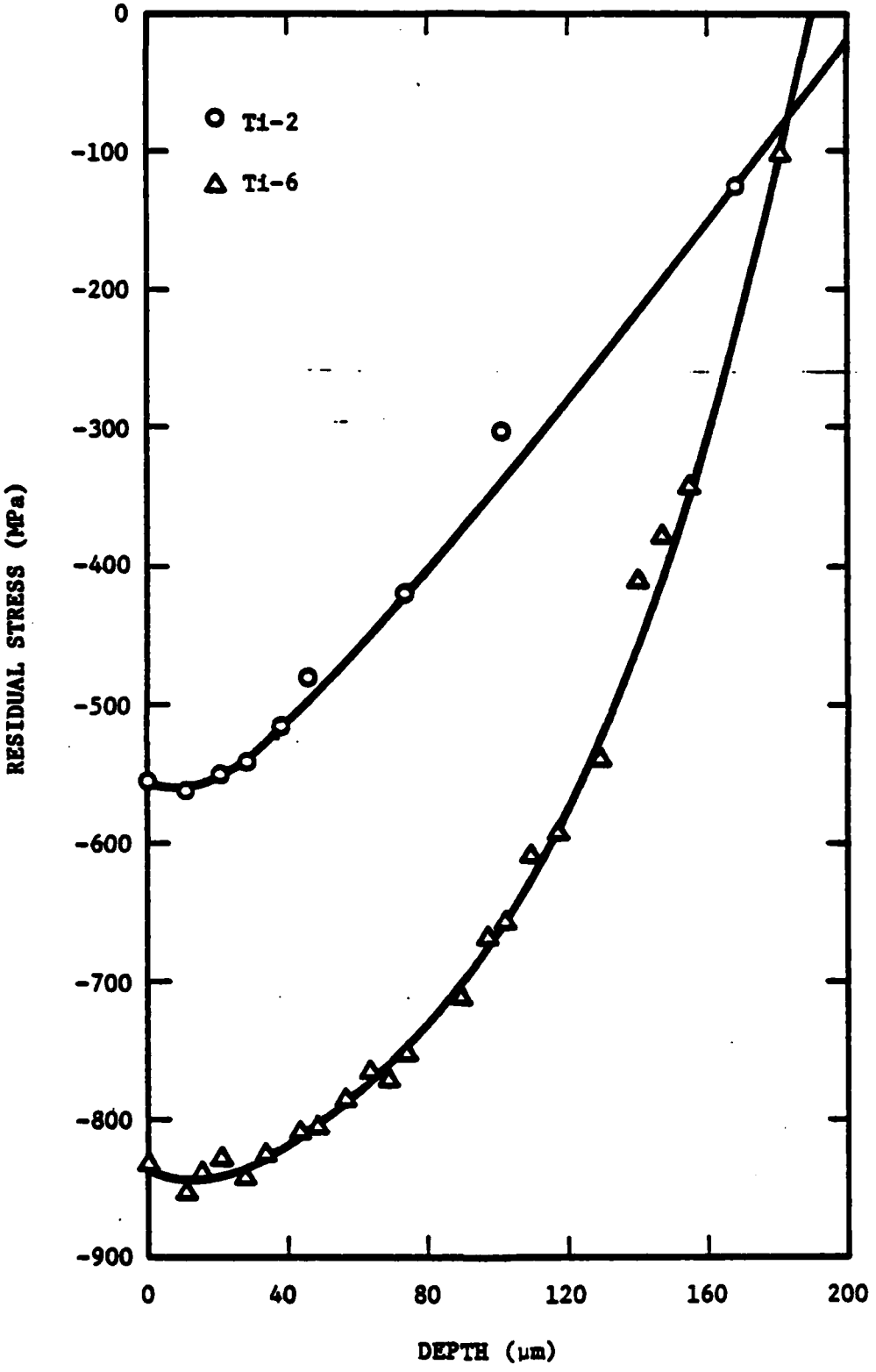

FIGURE 1. NEAR SURFACE RESIDUAL STRESS GRADIENTS IN CORNER-CRACKED Ti-6Al-4V SPECIMENS.

in a uniform field of a magnitude equivalent to that at the tip. The result would be a lenticular crack profile through the thickness which violates the geometry of the closed form solution.

In order to account for this discrepancy, another computer program, 3-D BINTEQ (Three-Dimensional Boundary Integral Technique)[6], was obtained. This program allows the direct calculation of crack surface displacements in the presence of residual stresses. This program also utilizes the boundary integral technique and served as the basis for the derivation of the influence functions for the various crack geometry options available in BIGIF. This relationship assured that the stress intensity factor and crack opening displacement calculations were performed in a consistent manner.

B. Results and Discussions

An appropriate elemental model for the corner crack in specimen Ti-6 (Table I) was formulated and computer runs were made with and without the actual compressive surface residual stress gradient measured in Ti-6 prior to the stress relief treatment. Results of calculations of the crack profiles for the two cases are compared in Figures 2a-f. In these figures, vertical displacements of the corner crack represent the opening of the crack due to an applied load of 56 MPa. Shaded regions indicate the interior portion of the crack face which is exposed due to the loading. The various rotated views show two major qualitative points. Firstly, the obvious point is that the presence of the compressive surface residual stress severely restricts the opening of the crack even though the major portion of the crack front has grown out of the zone of significant residual compression. A more subtle, yet more significant, result is that the

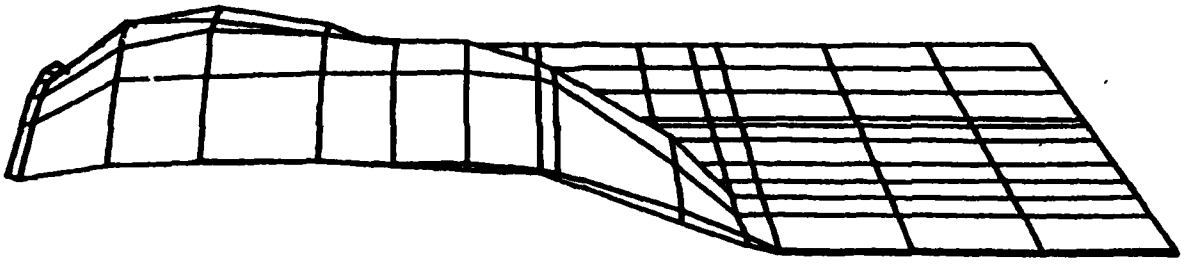

(a) Front Face View Before Stress Relief

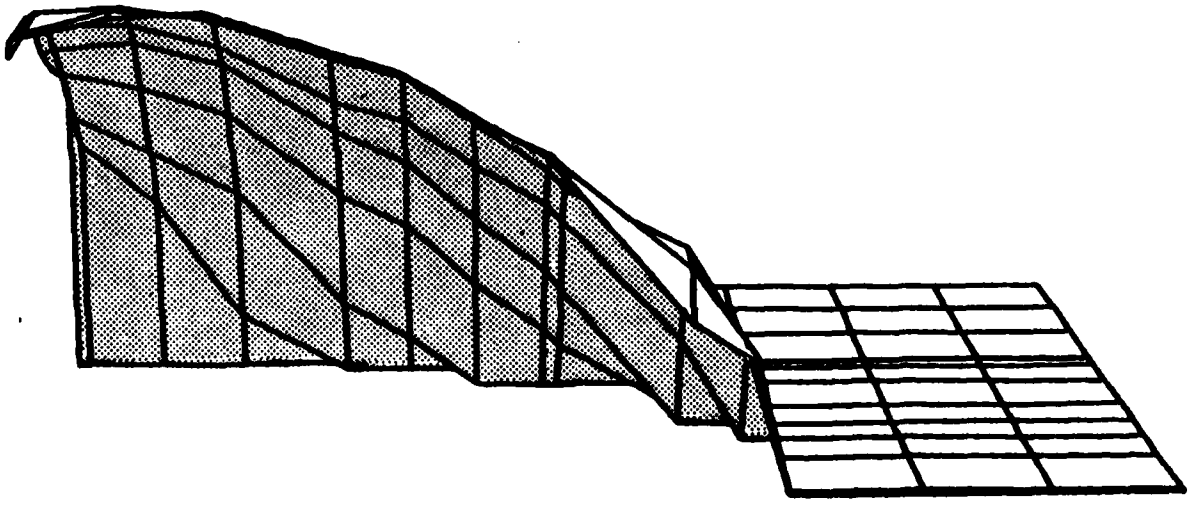

(b) Front Face View After Stress Relief

FIGURE 2. 3-D BINTEQ GENERATED THROUGH-THE-THICKNESS CRACK PROFILES FOR SAMPLE Ti-6. Shaded region indicates interior face of crack.

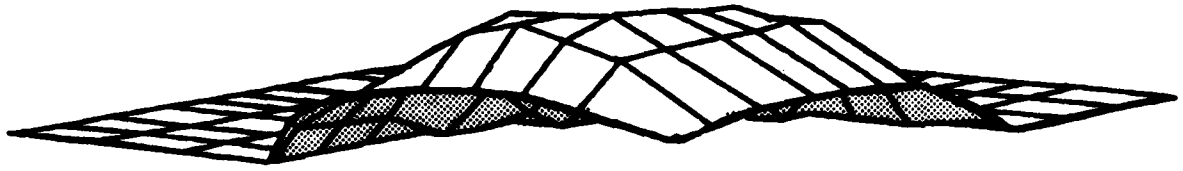

(c) Corner View Before Stress Relief

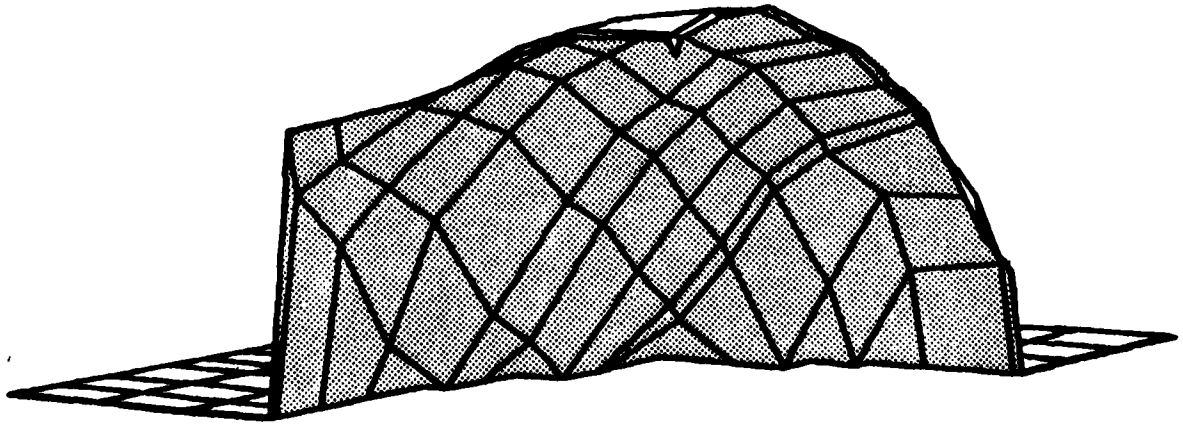

(d) Corner View After Stress Relief

FIGURE 2 (Continued). 3-D BINTEQ GENERATED THROUGH-THE-THICKNESS CRACK PROFILES FOR SAMPLE Ti-6. Shaded region indicates interior face of crack.

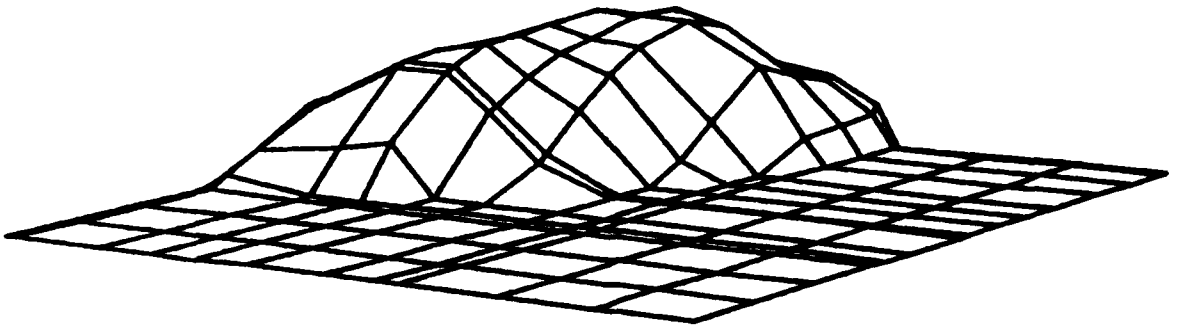

(e) Back View Before Stress Relief

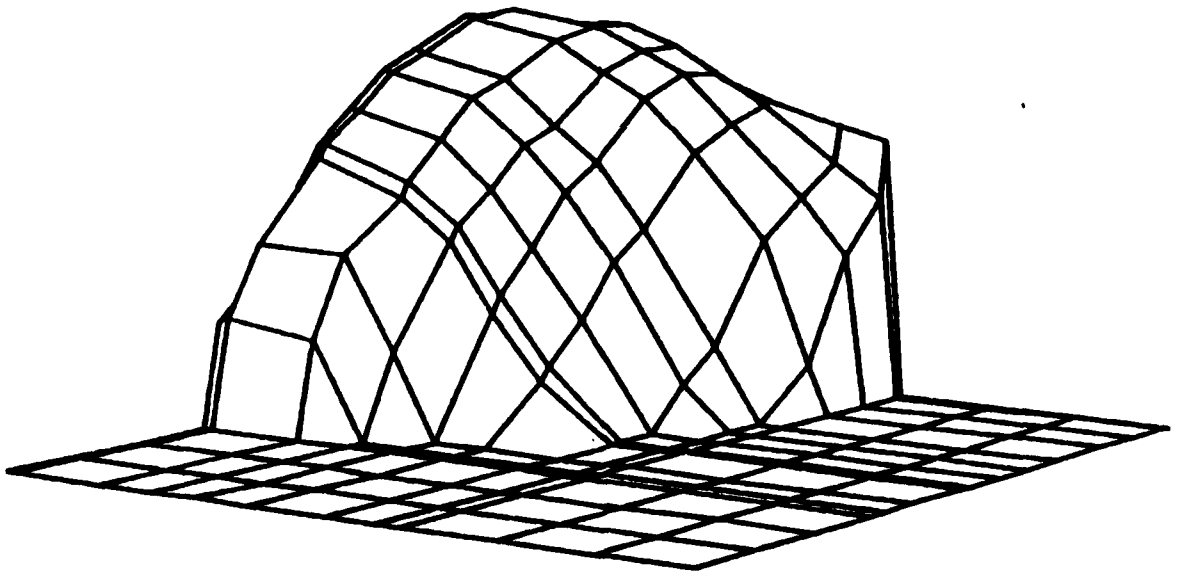

(f) Back View After Stress Relief

FIGURE 2 (Continued). 3-D BINTEQ GENERATED THROUGH-THE-THICKNESS CRACK PROFILES FOR SAMPLE Ti-6. Shaded region indicates interior face of crack.

through-the-thickness crack profile is nearly semi-elliptical in the stress-relieved condition but is lenticular when compressive surface residual stresses are present.

In addition to the qualitative observations made from the profile plots in Figures 2a-f, calculated values of the SCOD at the midpoint of the front crack face are compared with observed values in Table II. The data shows that not only does the boundary integral technique demonstrate the change in crack profile due to compressive surface residual stresses but also allows the quantification of the crack profile to a high degree of accuracy. Thus, the analytical approach developed on this program has proven to be a powerful tool for the prediction of crack opening behavior of large and small cracks under the influence of an imposed near-surface residual stress state. These results also add credibility to the stress intensity factors calculated by BIGIF in the presence of compressive surface residual stresses. In addition to the implications for such lifetime prediction efforts as retirement-for-cause, data in the next section shows that the compressive residual stress induced lenticular crack opening may also have a profound effect on the interaction of small cracks with aggressive environments.

TABLE II

CORRELATION OF MEASURED AND PREDICTED MODE I CORNER CRACK SCOD AT MAXIMUM LOAD IN SAMPLE Ti-6 USING 3-D BINTEQ

Surface Residual Stress Value, MPa	Maximum Applied Stress, MPa	K_s, MPa $\sqrt{m}$	Predicted SCOD, μm	Measured SCOD, μm
-860	560	9.6	2.6	3.1
≃0*	560	21.5	12.8	11.3

*Stress relieved after initial experiment.

III. CRACK OPENING AND GROWTH BEHAVIOR IN HY-130 STEEL

A. Experimental Procedure

Experiments were performed on HY-130 steel in both air and an aqueous solution of 3.5% NaCl. The HY-130 specimens were machined from a 50.8 mm rolled plate in the quenched-and-tempered condition. The alloy composition is summarized in Table III. The plate was provided by the David W. Taylor Naval Ship Research and Development Center through the auspices of the Office of Naval Research.

A cantilever beam fatigue specimen was used to promote surface crack initiation. Figure 3 shows the straight-sided specimen. A small, roughly semicircular starter notch (≈125μm long and 60μm deep) was placed in the center of the gage section by electrical discharge machining (EDM). It can be seen from the figure that slots are incorporated in the grip sections to allow for fixturing into the SEM tensile loading stage after the initiation of cracks in the bending rig.

The SEM loading stage, developed at SwRI [7] is shown in Figure 4. The stage is capable of cyclically loading a specimen in tension-tension at loads up to 3800N, at frequencies ranging from 0-5 Hz, while maintaining the area of interest within the viewing screen of the SEM and in focus. Crack behavior can be videotaped and replayed for analysis of crack opening displacement response. In addition, samples can be statically loaded in tension at loads up to 4900N.

Several HY-130 specimens were notched by EDM and precracked in bending between the strain limits of $0.15 \pm 0.25\%$. The specimens were subsequently

TABLE III

NOMINAL COMPOSITION OF HY-130

Element	Wt - Pct
C	0.12
Mn	0.60 - 0.90
P (max)	0.01
S (max)	0.015
Si	0.20 - 0.35
Ni	4.75 - 5.25
Cr	0.40 - 0.70
Mo	0.30 - 0.65
V	0.05 - 0.10

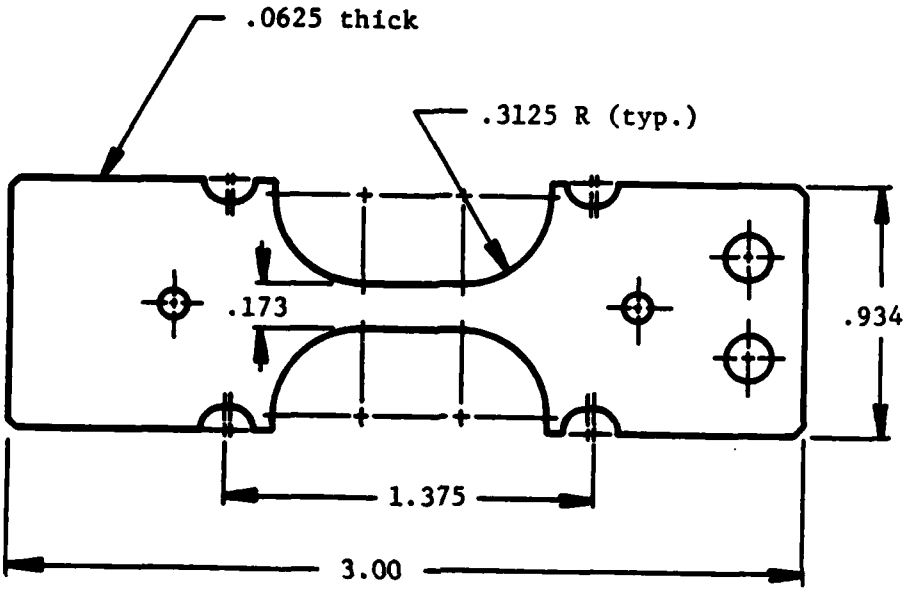

FIGURE 3. SPECIMEN DESIGN. All dimensions in inches.

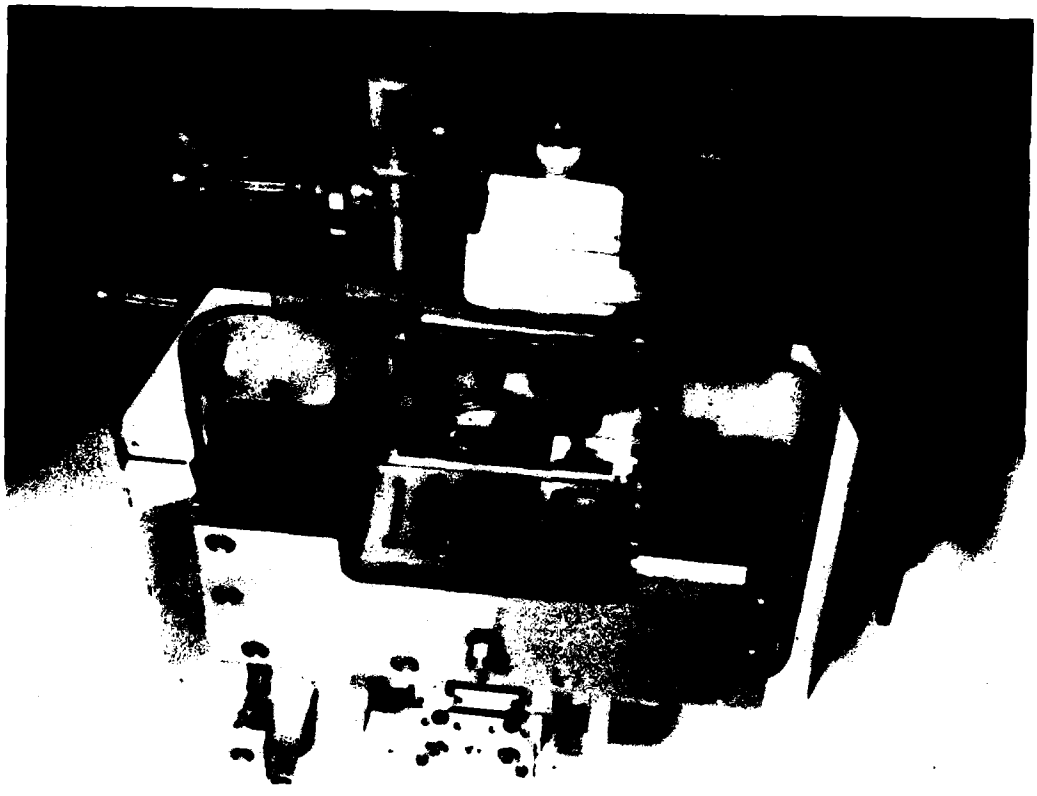

FIGURE 4. IN-SITU LOADING STAGE FOR SEM.

shot-peened on both sides at an intensity of 0.011A. This was followed by a metallurgical polish to remove the EDM notch while leaving the small surface crack which had initiated at the base of the notch. The samples were polished on both the front and back surfaces to prevent bowing. An example of one of the cracks obtained in this manner is shown in Figure 5.

The d vs. $\sin^2 \psi$ X-ray diffraction technique [8] was used to measure the surface residual stress level on all of the specimens. A computer program developed earlier in this project was used to perform a second-degree curve fit to the intensity vs. 2θ data obtained from the X-ray stress measurements. Enough points are used to determine the peaks of interest at ψ = 0, 15, 30 and 45°; then the peak positions and d spacings are calculated. The slope of d vs. $\sin^2 \psi$ is obtained and used to calculate the residual stress. The coefficient of correlation for the linear curve fit is generally in the range of 97-99%, indicating a high degree of accuracy in the measurements. A residual stress profile for one of the specimens, HY-18, was obtained by repetition of the residual stress measurements after successive removal of layers of material by electropolishing. The data obtained in this manner were subsequently corrected for beam penetration and layer removal effects by standard procedures [9,10]. Measurements of the near-surface residual stress gradients for the other HY-130 specimens are currently under way.

Receiving slits of 1° and 0.018° and primary beam slits of 1° were used for all measurements. No Soller slits were used and the measurements for all peaks were performed with the detector at a fixed position. $C_r K_\alpha$ radiation with a vanadium oxide filter was used in conjunction with the (211) plane for the steel specimens. The value of $E/(1 + \nu)$ used in the stress calculations was 1.59×10^5 MPa [11].

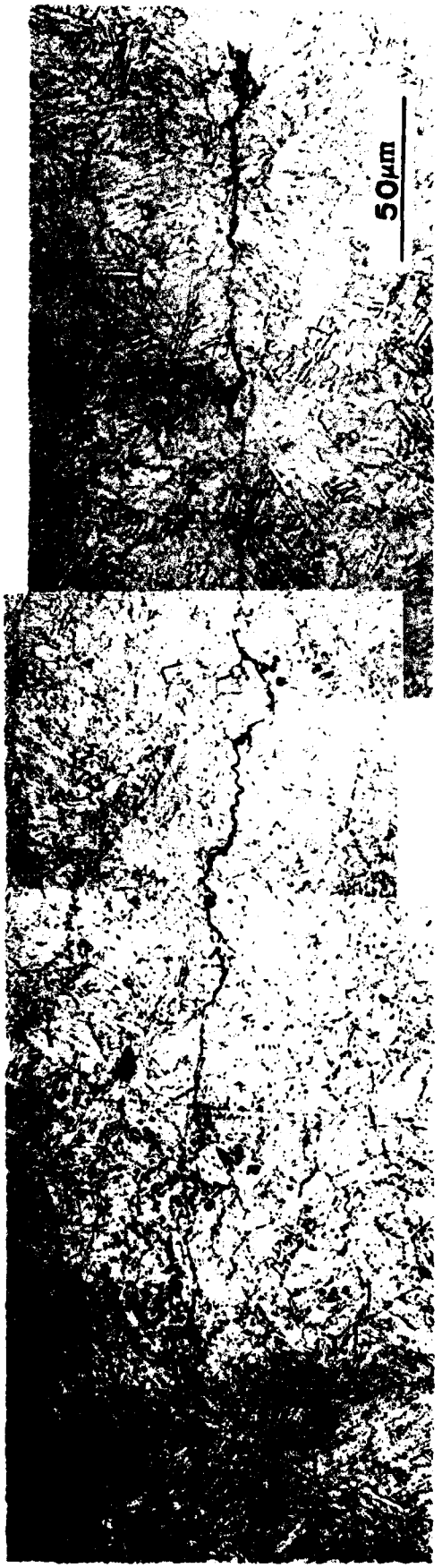

FIGURE 5. INITIAL CRACK IN SAMPLE HY-15.

All testing was performed at room temperature. Prior to the initial examination of the SCOD behavior, the samples were subjected to several hundred cycles under load control in axial tension in the SEM stage. Load limits used were ≃ 100-700 MPa for the HY-130. Both static and dynamic measurements of the SCOD vs. load behavior were performed on the specimens. Dynamic observations were made at a cyclic frequency of 1 Hz. The surface cracks were then grown approximately 50 μm in total length along the surface in a laboratory air environment at a frequency of 1 Hz and an R-ratio of 0.1. After the SCOD measurements were repeated, the cracks were grown again in an aqueous solution of 3.5% NaCl. Then SCOD measurements were performed again. This procedure relies on the observation of Davidson that environmentally induced crack tip plasticity and opening behavior persists during a transient period after the environment is removed [12].

After all the measurements were taken, the specimens were broken open to reveal the crack geometry. By careful examination of the fracture surface, the depth profiles of the cracks at the three measurement points could be detected. An example is given in Figure 6. These geometries and the applied loads were used to calculate the stress intensity factors at the buried (K_B) and the surface (K_s) crack tips using BIGIF. In addition, the average stress intensity range and crack depth and length changes for the various growth cycles were established. These data were used to obtain plots of stress intensity range vs. crack growth rate for the surface and buried portions of the cracks.

B. Results and Discussion

A summary of crack geometry, surface residual stress and calculated stress intensity data is shown in Table IV for all the specimens studied.

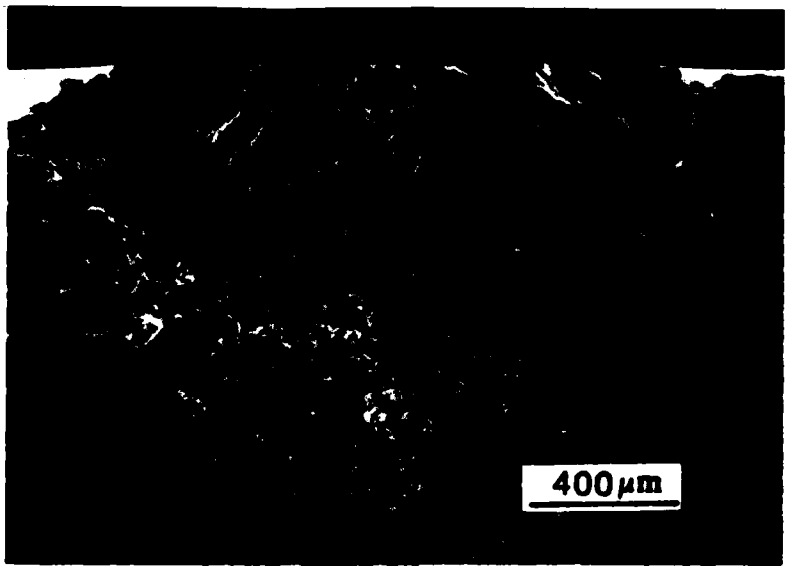

FIGURE 6. CRACK SURFACE IN SAMPLE HY-18. Arrows indicate position of crack front in initial condition and after growth in air.

TABLE IV

SUMMARY OF CRACK GEOMETRY AND STRESS STATE DATA
FOR ALL HY-130 SPECIMENS

Sample	Condition	C (μm)	$\frac{a}{c}$	Surface Residual Stress (MPa)*	K_B (MPa $\sqrt{m}$)	K_S (MPa $\sqrt{m}$)
HY-15	Initial	.50	.28	- 91	8.2	6.4
	After Air	.75	.48	- 91	10.6	9.1
	After NaCl	.83	.91	- 91	12.2	12.3
HY-17	Initial	.35	.50	-120	9.4	8.1
	After Air	.52	.58	-120	10.4	9.3
HY-20	Initial	.91	.31	-130	9.5	7.5
	After Air	216	.61	-130	12.5	11.3
	After NaCl	244	.79	-130	13.9	13.4
HY-23	Initial	188	.31	-194	9.7	7.7
	After Air	191	.44	-194	10.8	9.1
	After NaCl	198	.46	-194	11.2	9.5
HY-18	Initial	622	.57	-297**	16.7***	12.7***
	After Air	648	.82	-297**	19.4***	17.0***
	After NaCl	668	.93	-297**	20.2***	18.4***

*Uncorrected for beam penetration.

**Corrected for beam penetration.

***Corrected for residual stress gradient.

As can be seen from the data, the half-crack length ranged from 130-620 μm for the specimens in the initial condition. Crack depths ranged from 50-350 μm. Compressive surface residual stresses remaining in the specimens after polishing were on the order of 90-325 MPa. These values did not change significantly during cycling. Also, the stress intensity factors at 689 MPa ranged from 6.5-20 MPa μm. The stress intensities at the buried crack tips were slightly higher than those found at the surface crack tips. This is due to the change in loading from bending to axial which induces a slight amount of crack tunnelling until the new equilibrium shape is achieved. The K_B and K_S data for specimen HY-18 are corrected for the rather significant compressive residual stress gradient present at the surface of this specimen. This profile is shown in Figure 7, corrected for beam penetration and layer removal. The profile was incorporated into the BIGIF stress intensity calculations using a piecewise linear approximation.

Examples of SCOD behavior as a function of load are given in Figures 8-10. It can be seen from the figures that as the level of surface compressive stress increases, opening of the crack is delayed. This is analogous to what was reported earlier in Ti-6Al-4V. Also, in general, as the cracks become larger and K increases, the crack opening increases for a given applied load. The aqueous brine environment does not appear to significantly affect crack opening behavior.

Table V summarizes the observed crack opening behavior at 689 MPa and gives a comparison with predictions based upon the closed form solution described in the previous section. The data shows that at small levels of residual compression on the order of 100 MPa, the closed form solution

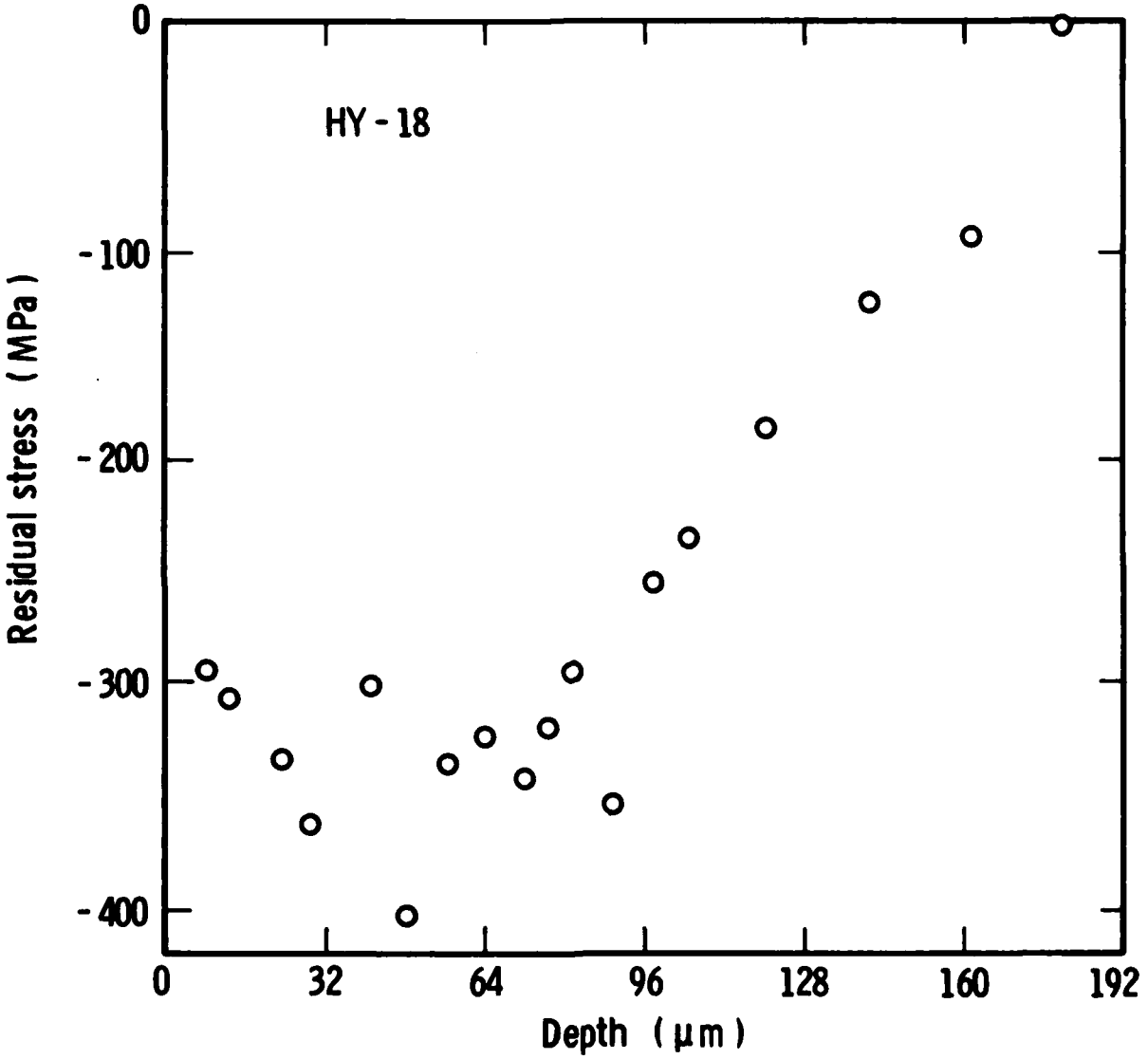

FIGURE 7. NEAR-SURFACE RESIDUAL STRESS PROFILES IN SAMPLE HY-18 (CORRECTED FOR BEAM PENETRATION AND LAYER REMOVAL).

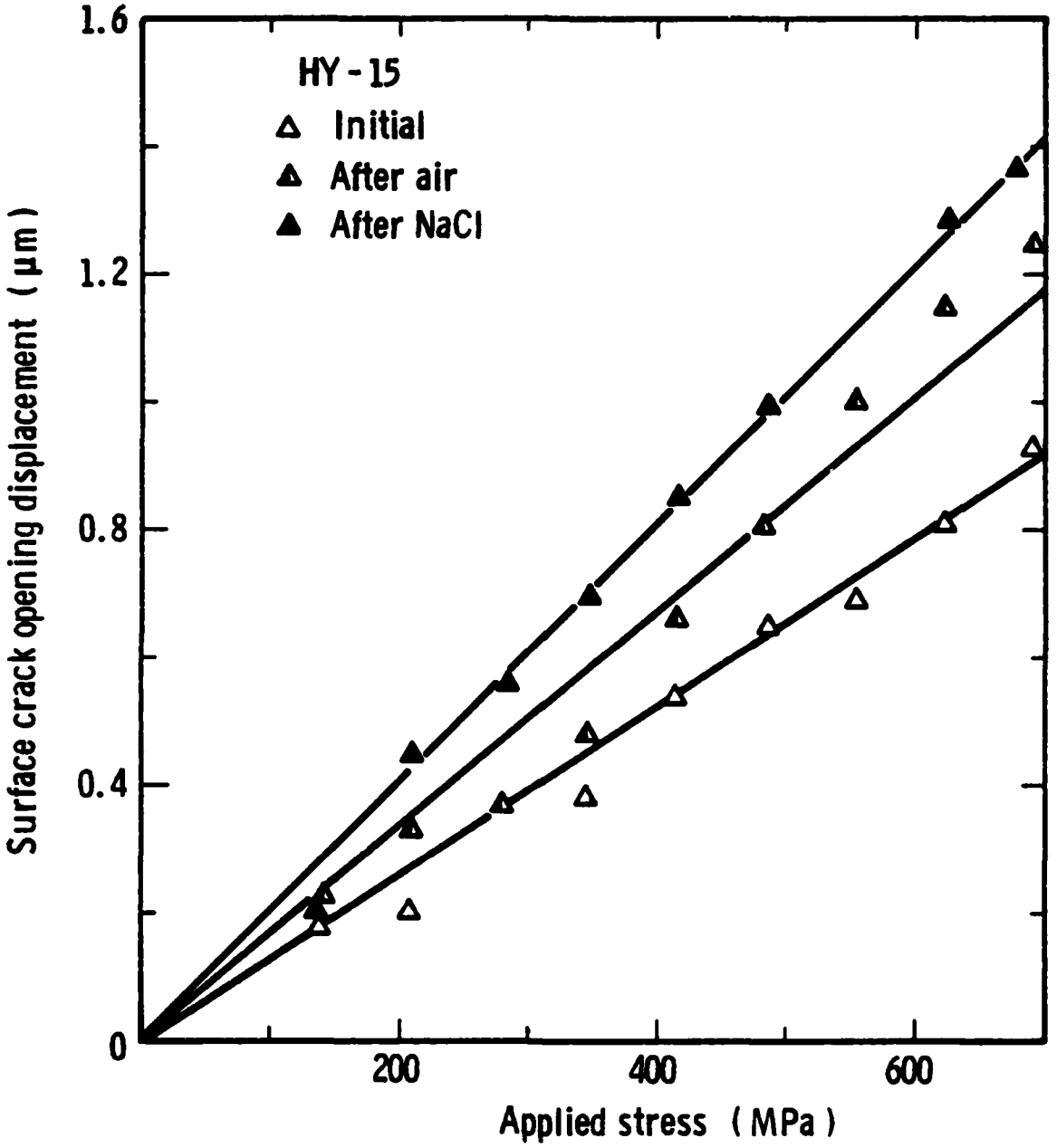

FIGURE 8. SCOD VS. STRESS DATA FOR SAMPLE HY-15.

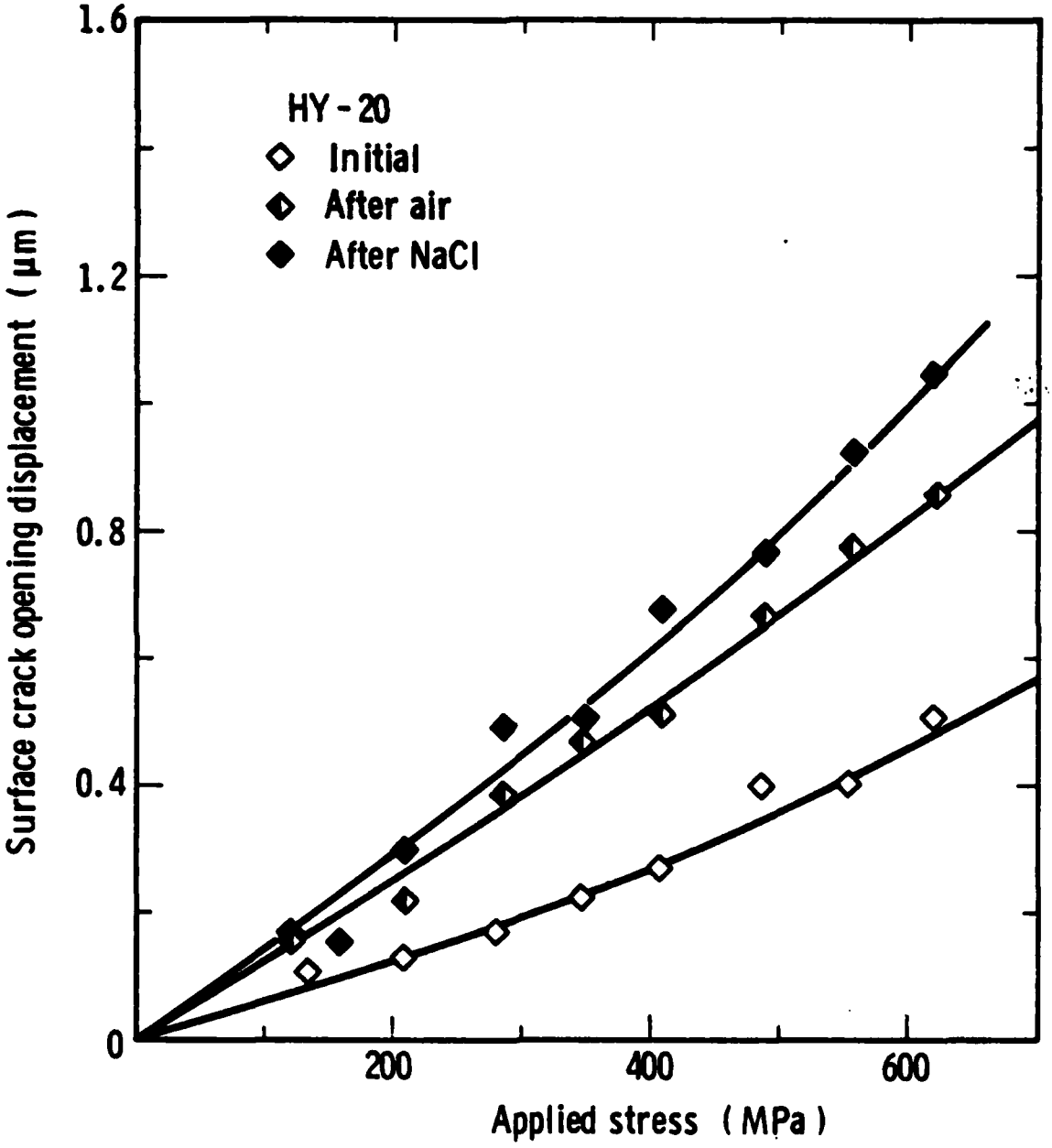

FIGURE 9. SCOD VS. STRESS DATA FOR SAMPLE HY-20.

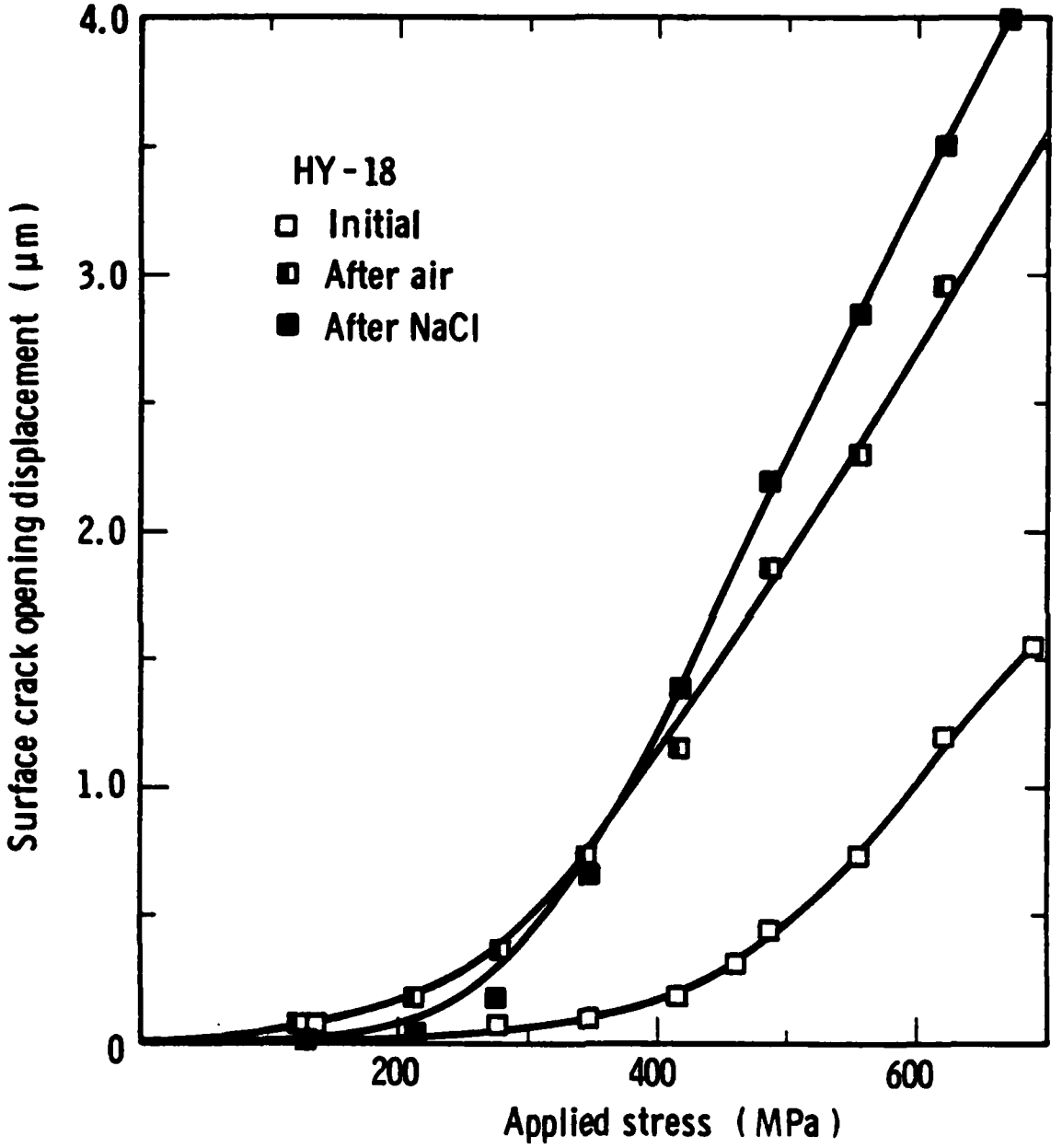

FIGURE 10. SCOD VS. STRESS DATA FOR SAMPLE HY-18.

TABLE V

SUMMARY OF MEASURED AND PREDICTED SCOD BEHAVIOR AT 689 MPa

Sample	Condition	Surface Residual Stress (MPa)*	Measured SCOD (μm)	Predicted SCOD (μm)
HY-15	Initial	- 91	.91	.76
	After Air	- 91	1.24	1.17
	After NaCl	- 91	1.40	1.61
HY-17	Initial	-120	.75	.92
	After Air	-120	1.30	1.11
HY-20	Initial	-130	.53	1.01
	After Air	-130	.96	1.61
	After NaCl	-130	1.16	2.03
HY-23	Initial	-194	.80	1.02
	After Air	-194	.66	1.22
	After NaCl	-194	.75	1.30
HY-18	Initial	-297**	1.56***	3.08***
	After Air	-297**	3.95***	4.19***
	After NaCl	-297**	4.82***	4.61***

*Uncorrected for beam penetration.

**Corrected for beam penetration.

***Corrected for residual stress gradient.

predicts the SCOD quite well. In addition, the presence of the aqueous brine environment does not affect the prediction of the crack opening behavior. At levels of residual compressive stress greater than about 130 MPa, opening behavior does become influenced by the residual stress and this is reflected in the failure of the closed form solution. The closed form solution leads to an overprediction of the observed SCOD even in the initial case for Sample HY-18, where the K data was corrected for the large stress gradient. It is interesting to note, however, that as the relatively large surface crack in Sample HY-18 doubled its depth during the air and brine growth increment, the influence of the compressive surface residual stress lessened. In fact, the closed form solution came very close to predicting the actual opening of the enlarged crack in HY-18 when residual stresses were accounted for in the K calculations. This implies that the crack was large enough after the growth increments to be relatively free of the constraint of the residual stress. Prior experience with the Ti-6Al-4V specimens described in the previous section indicates that the surface microcracks in the steel specimens with significant surface compressive residual stresses are also opening in a lenticular fashion through the thickness of the specimen. Calculations of crack openings for selected HY-130 specimens are currently underway using 3-D BINTEQ and the actual residual stress gradient to verify this point.

Crack growth data along the surface of the specimen (dc/dn) are summarized in Figure 11 for both air and brine environments. Also included are independent data for large cracks [13] and small cracks [14] in air and brine. As can be seen from the data, except for the points from

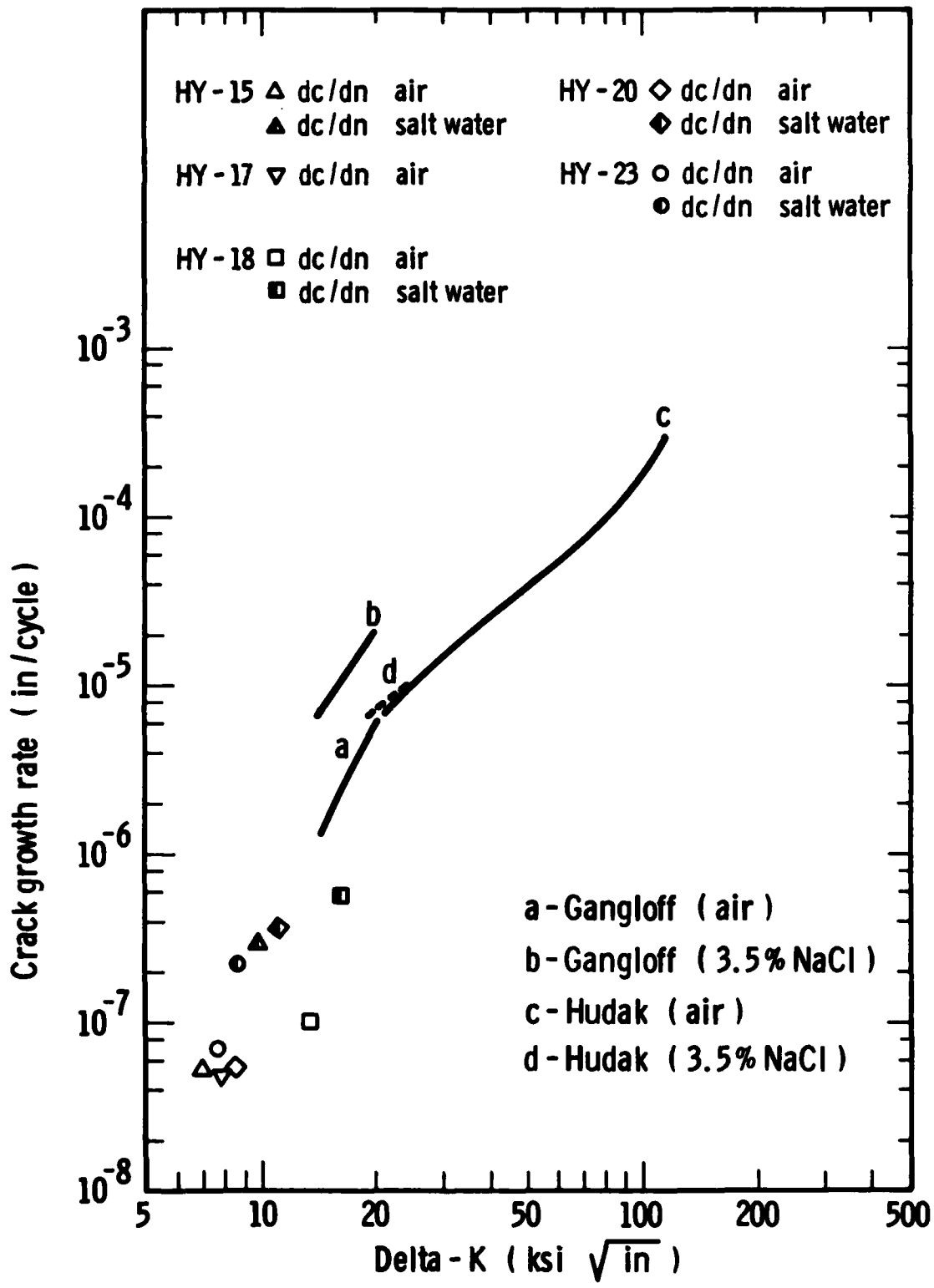

FIGURE 11. COMPARISON OF dc/dn VS. ΔK DATA FOR ALL HY-130 SPECIMENS WITH INDEPENDENT DATA FOR SMALL CRACKS (GANGLOFF [14]) AND LARGE CRACKS (HUDAK [13]).

HY-18, all the experimental points fall on an extension of the data of Hudak and Gangloff for large and small cracks in air. This is consistent with observations by Gangloff that small cracks do not show accelerated surface growth in a brine environment [15]. Figure 12 repeats the dc/dn data but also includes crack growth data for growth into the specimen (da/dn). It can be seen that da/dn is also unaffected by the presence of the brine environment when the SCOD behavior is affected by the residual stress. However, in the case of HY-15, where the slight amount of residual compression at the surface did not retard crack opening, there is a distinct acceleration in da/dn in a brine environment consistent with that found by Gangloff [14].

The accelerated crack growth of small cracks in steel in brine environments has been explained by the inefficiency of small cracks in pumping fresh, aerated fluid to the crack tip. Large cracks pump large amounts of fluid which promote mixing of the solution at the crack tip. This not only destroys any accumulation of free hydrogen at the crack tip, but also tends to poison the formation of free hydrogen [16]. Since the near surface region of a small semielliptical crack is not nearly as occluded as the buried crack front, the effect on crack growth rate would not be expected to be as significant for dc/dn as it would be for da/dn. This is reflected in the data. However, the data also indicates that the presence of a compressive residual stress field exerts more than a purely mechanical effect on crack growth behavior. Realizing that a compressive residual stress induces lenticular crack opening through the thickness of the specimen, it

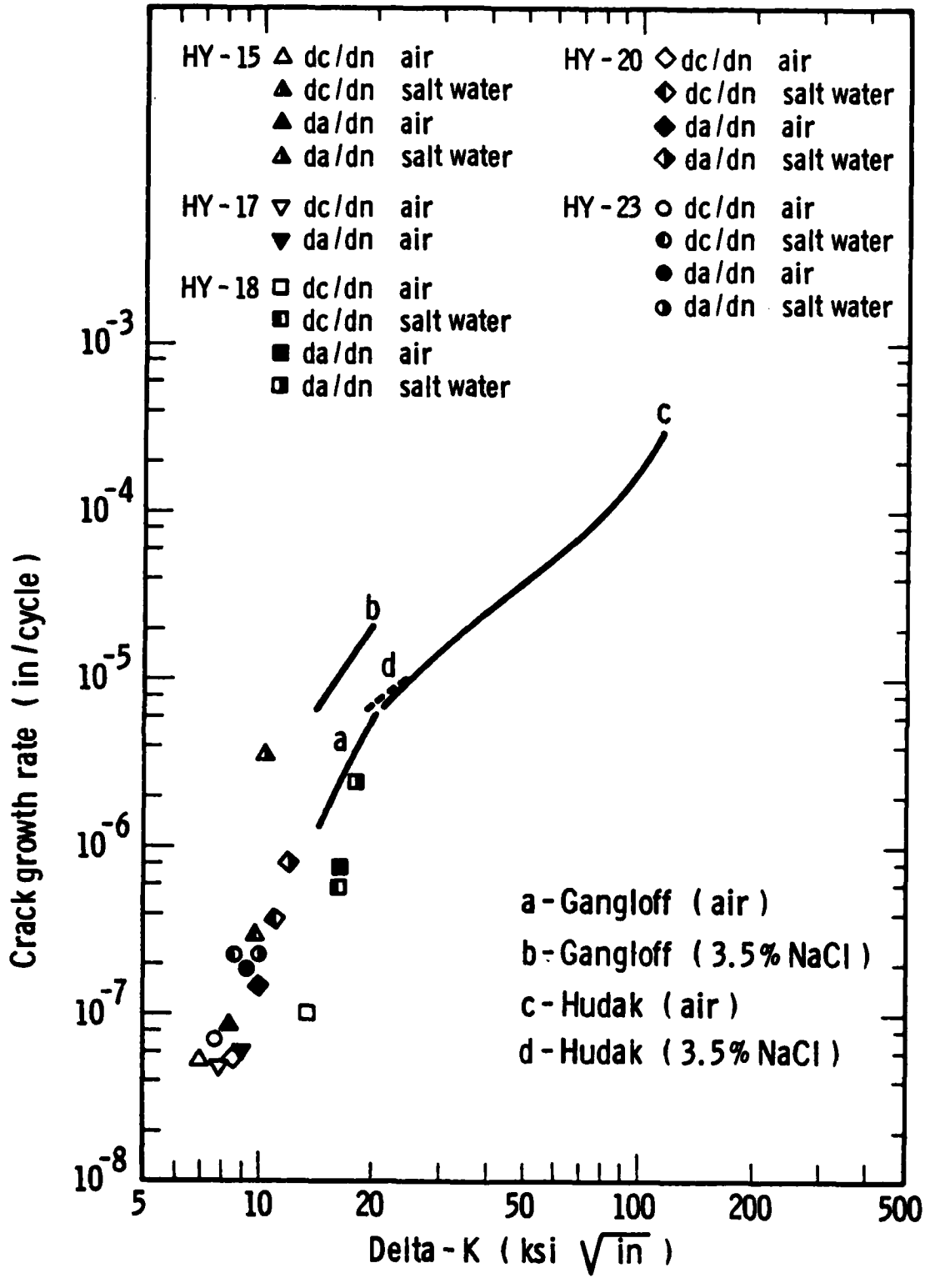

FIGURE 12. COMPARISON OF dc/dn AND da/dn VS. ΔK DATA FOR ALL HY-130 SPECIMENS WITH INDEPENDENT DATA FOR SMALL CRACKS (GANGLOFF [14]) AND LARGE CRACKS (HUDAK [13]).

is likely that a small vacuum would be produced within such a crack during the opening event. This would act to draw fluid into the crack very quickly and create a great deal of turbulence. This turbulence would promote mixing of the fluid within the crack, thus reducing the deleterious effect of the brine environment by the mechanisms described above. Initial treatment of fluid flow behavior in small cracks due to crack closure by Gangloff [17] agrees with this hypothesis.

It should be noted that, except for the data for HY-18, the stress intensities plotted in Figures 11 and 12 have not yet been corrected for any residual stress effects. However, at the levels of K used in these experiments, very little shift to lower effective ΔK values will be induced by this correction. Calculations are currently under way to perform this slight adjustment in the growth rate curves. Also, the strong effect of residual stress on growth rate in Sample HY-18, even after correction for the large value of residual compression, is not well understood at this time.

IV. MICROSTRUCTURAL DEVELOPMENT IN THICK TI ALLOY WELDMENTS

A. Background

Three one-inch thick welded panels of Ti-6Al-2Nb-1Ta-0.8Mo (Ti-6211) were obtained through Dr. Bruce MacDonald of the Office of Naval Research and Mr. Ivan Caplan and Dr. William Lukens of the David Taylor Naval Ship Research and Development Center. The panels measured 18" x 28" with the weld in each running lengthwise along the center of the panel. The three panels represented samples of a typical standard gas-metal arc weld (GMA), extended electrode gas-metal arc weld (EE) and a deep gas-tungsten arc weld (DTIG). The eventual goals of this task are to establish the effects of residual stress state and microstructure on fatigue crack growth behavior in these welded materials. Initial efforts have been expended on the characterization of the residual stress state and microstructure in the weld and heat-affected zones. To date relaxation of strain gages during cutting of the plates and optical metallography have been the primary tools used.

B. Results and Discussion

Resistance type strain gages were attached at various positions across the welds and were monitored during the cutting of the panels. Initial relaxation data indicates that the level of tensile residual stress in the near weld region is substantial (on the order of 350-550 MPa) in the EE and DTIG welds. X-ray residual stress measurements of surface stresses and two-dimensional profiles are currently being planned.

Macrographs of the three weld types are shown in Figures 13-15. One qualitative note from the macrographs is that epitaxial growth is seen across remelt zones in the GMA and EE welds but not in the DTIG weld. Higher magnification shots of the three weld and heat-affected zones are presented in Figures 16 and 17, respectively. The microstructure of the DTIG weld zone consisted of a fine colony structure of aligned alpha platelets with a film of beta phase at the platelet boundaries. The fusion zones of the GMA and EE welds appear to be a fine basketweave structure of acicular alpha phase. The heat-affected zones in all three welds consist of extremely fine acicular alpha phase. It should be noted that it is very difficult to differentiate between acicular alpha phase and the hcp alpha prime martensite phase by optical metallography. A more accurate determination of the structure in the weld zones of the three processes is currently being conducted by electron diffraction on thin foils. The large colony structure of the base metal plates is also being characterized by transmission electron microscopy.

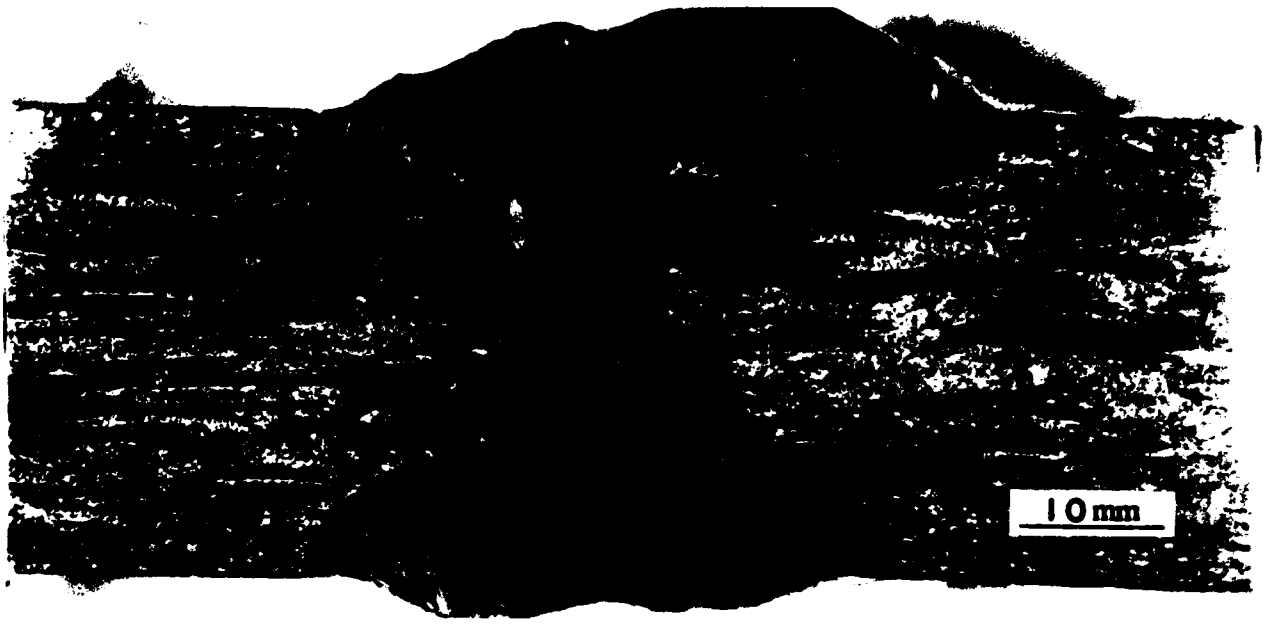

FIGURE 13. MACROGRAPH OF GAS-METAL ARC WELD (GMA).

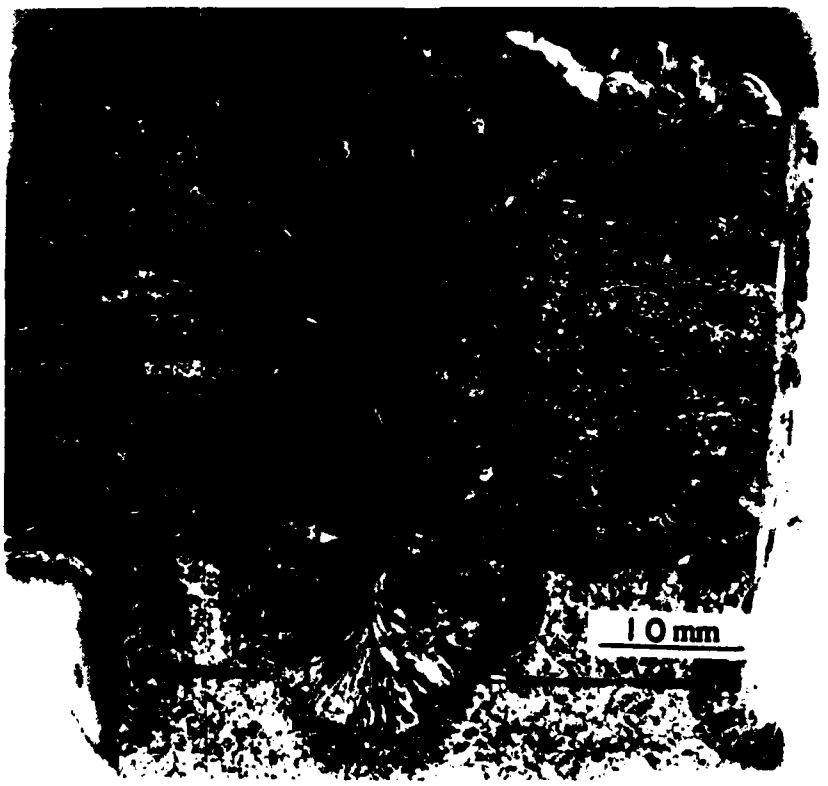

FIGURE 14. MACROGRAPH OF EXTENDED ELECTRODE WELD (EE).

FIGURE 15. MACROGRAPH OF DEEP GAS-TUNGSTEN ARC WELD (DTIG).

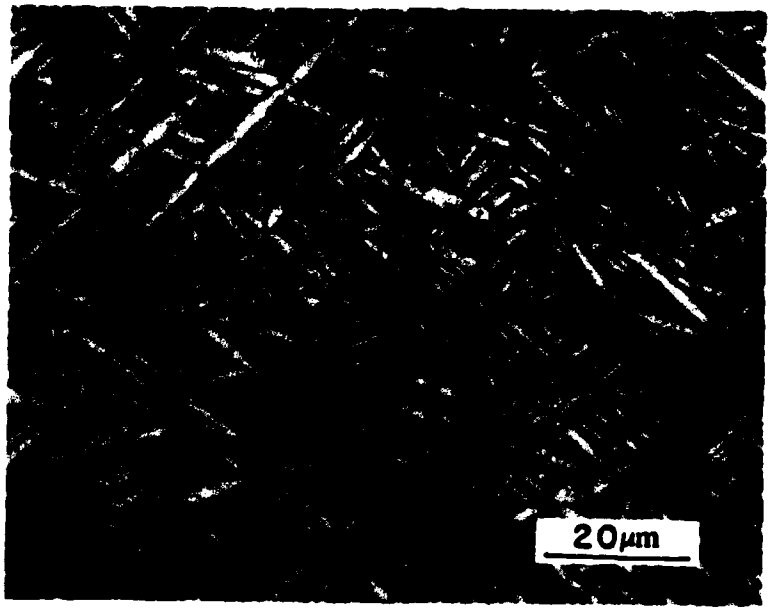

(a) Gas-Metal Arc

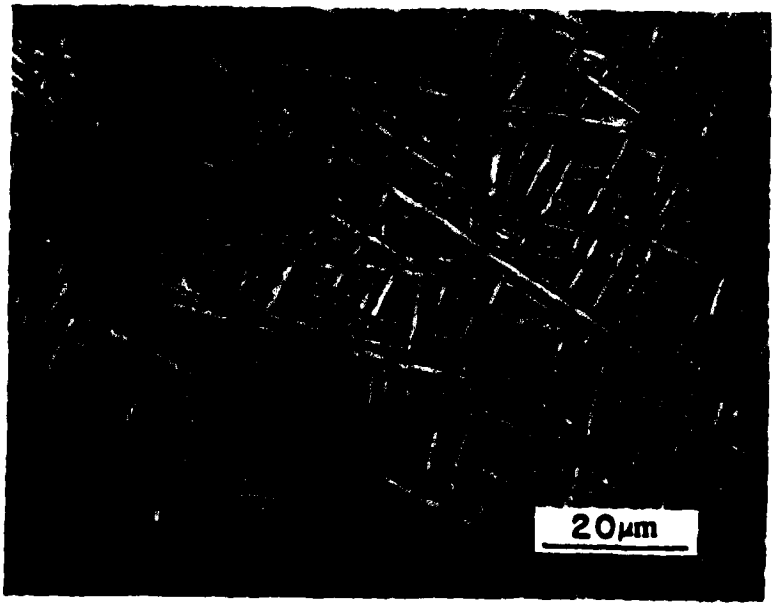

(b) Extended Electrode

FIGURE 16. MICROSTRUCTURES OF THE WELD REGIONS OF THE THREE TYPES OF WELDS.

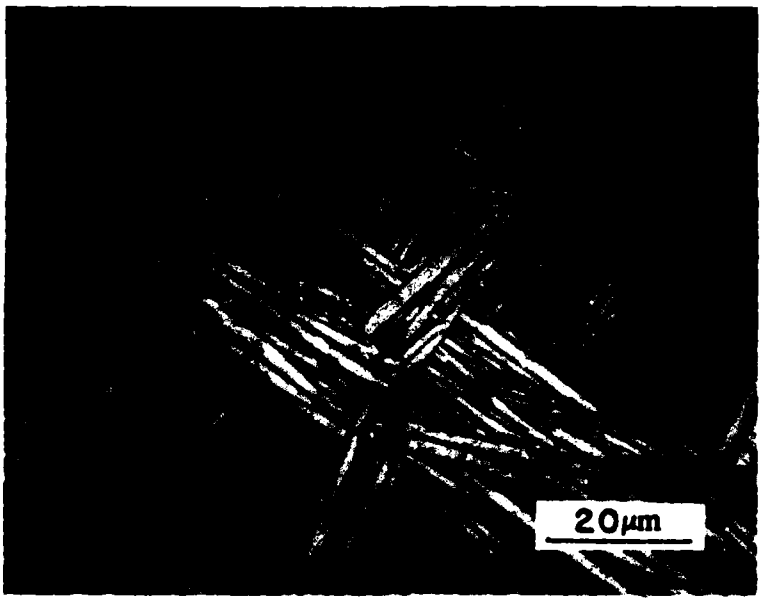

(c) Deep Gas-Tungsten Arc

FIGURE 16 (Continued). MICROSTRUCTURES OF THE WELD REGIONS OF THE THREE TYPES OF WELDS.

(a) Gas-Metal Arc

FIGURE 17. MICROSTRUCTURES OF THE HEAT-AFFECTED ZONES OF THE THREE TYPES OF WELDS.

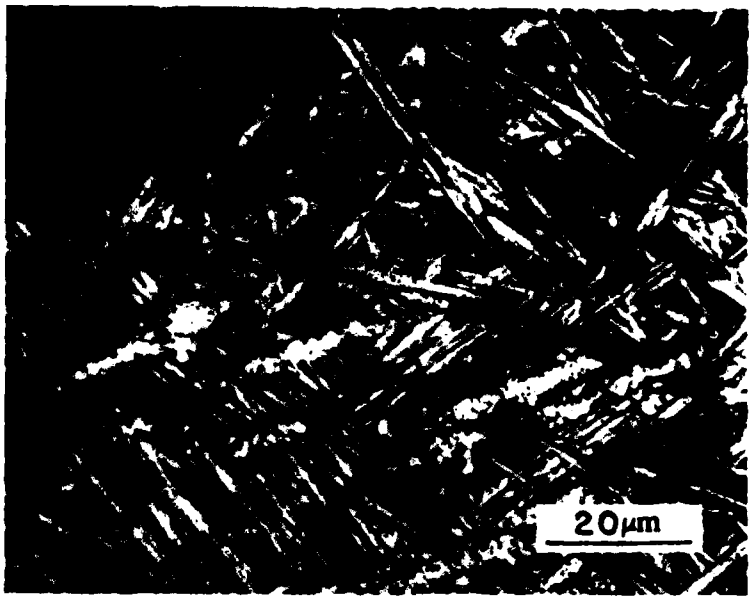

(b) Extended Electrode

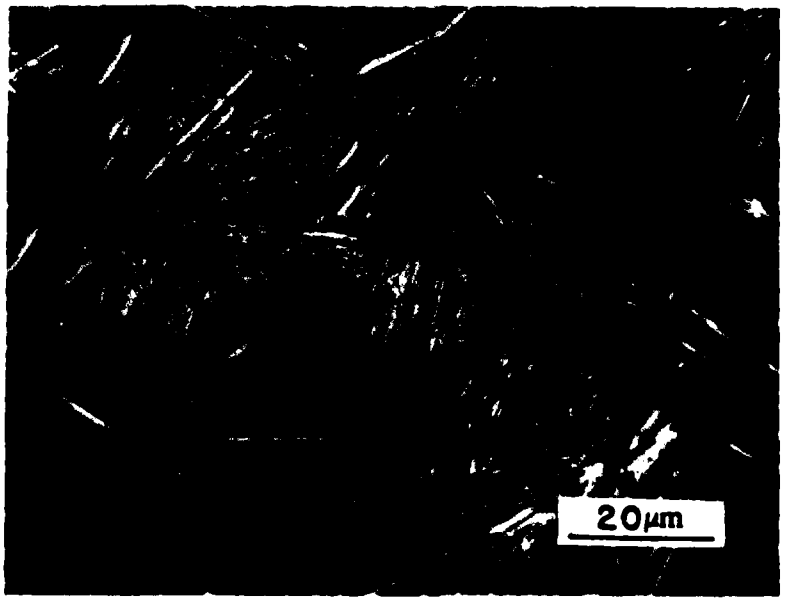

(c) Deep Gas-Tungsten Arc

FIGURE 17 (Continued). MICROSTRUCTURES OF THE HEAT-AFFECTED ZONES OF THE THREE TYPES OF WELDS.

V. CONCLUSIONS

(1) Surface compressive residual stresses can induce lenticular opening of small part-through cracks through-the-thickness of a specimen.

(2) This lenticular opening behavior can be predicted by the use of the boundary integral technique. The excellent agreement between observed and predicted opening behavior provides a great deal of confidence in crack tip stress intensity values which are also calculated by this technique.

(3) In addition to a purely mechanical effect on the reduction of crack tip stress intensity, the lenticular crack opening behavior induced by surface compressive residual stresses apparently decreases the crack growth rate of small cracks in a brine solution by disrupting the evolution and/or accumulation of hydrogen at the crack tip.

VI. REFERENCES

1. A. J. McEvily and T. L. Johnston, Int. J. Frac. Mech., Vol. 3, 1967, p. 45.

2. G. G. Garrett and J. F. Knott, Met. Trans., Vol. 7A, 1976, p. 884.

3. J. E. Hack and G. R. Leverant, in Residual Stress Effects in Fatigue, ASTM STP 776, 1982, p. 204.

4. G. R. Irwin, J. Appl. Mech., December 1962, p. 651.

5. P. M. Besuner, D. C. Peters and R. C. Cippola, BIGIF Fracture Mechanics Code for Structures, Key Phase Report, NP-838 Research Project 700-1, EPRI, July 1978.

6. T. A. Cruse, An Improved Boundary Integral Equation Method for Three-Dimensional Elastic Stress Analysis, Interim Report on Contract DA-ARO-D-31-124-72-G3, Carnegie-Mellon University, August 1973.

7. D. L. Davidson and A. Nagy, J. Phys. E. (Sci. Inst.), Vol. 11, 1978, p. 207.

8. E. Macherauch, Exp. Mech., Vol. 6, 1966, p. 140.

9. SAE Information Report TR182, A. L. Christensen, Ed., 1960.

10. M. G. Moore and W. P. Evans, SAE Trans., Vol. 66, 1958, p. 340.

11. A. L. Christenson and E. S. Rowland, Trans. of ASM, Vol. 45, 1953, p. 638.

12. D. L. Davidson and J. Lankford, Jr., Int. J. Fracture, Vol. 17, June 1981, p. 257.

13. S. J. Hudak, Jr., Unpublished Research, Southwest Research Institute, San Antonio, Texas, 1982.

14. R. P. Gangloff, Unpublished Research, Exxon Research and Engineering Company, Linden, New Jersey, 1982.

15. R. P. Gangloff, Fat. of Eng. Mat. and Struct., Vol. 4, 1981, p. 15.

16. R. P. Gangloff, "The Criticality of Crack Size in Aqueous Corrosion Fatigue," submitted for publication in Res. Mechanica Letters, 1982.

17. R. P. Gangloff, private communication, Exxon Research and Engineering Company, Linden, New Jersey, 1982.